Flux-noise spectra around the Kosterlitz-Thouless transition for two-dimensional superconductors

Beom Jun Kim and Petter Minnhagen
Department of Theoretical Physics, Umeå University, 901 87 Umeå, Sweden

(Received 9 February 1999)

The flux-noise spectra around the Kosterlitz-Thouless transition are obtained from simulations of the two-dimensional resistively shunted junction model. In particular the dependence on the distance d between the pickup coil and the sample is investigated. The typical experimental situation corresponds to the large-d limit and a simple relation valid in this limit between the complex impedance and the noise spectra is clarified. Features, which distinguish between the large- and small-d limit, are identified and the possibility of observing these features in experiments is discussed. [S0163-1829(99)04130-2]

I. INTRODUCTION

Spontaneously created vortices drive the transition between the superconducting and normal state for thin-film superconductors and two-dimensional (2D) Josephson-junction arrays (JJA's).[1] This means that the physics of the vortices is responsible for the characteristic features in a region around the transition. One manifestation of this is the static characteristics of the phase transition which is of the Kosterlitz-Thouless (KT) type.[1,2] Another manifestation is the dynamical features around the transition. These are reflected in the flux-noise spectra and the complex impedance. In this paper we investigate the flux-noise spectra through computer simulations of the resistively-shunted Josephson-junction (RSJ) model on a 2D square lattice. In particular we clarify the relation between the flux-noise spectra and the complex impedance.

There have been a number of recent experimental[3–6] as well as theoretical studies[7–12] dealing with the flux-noise spectra. The typical experimental setup measures the fluctuation of the magnetic flux through a pickup coil situated at a distance above the sample.[3–6] Many simulation studies, on the other hand, have measured the vorticity fluctuation associated with a fixed area of the sample itself.[8–10] It has been assumed that this would roughly correspond to the magnetic flux spectra of the experiments. However, in the present investigation we show that there are significant differences. The typical experimental situation corresponds to the limit of large distance between the pickup coil and the sample. In this limit there exists a simple relation[7] between the flux-noise spectra and the complex impedance of the sample, which we here verify both directly from the simulations and through analytic calculations.

In Sec. II we describe how the flux-noise spectrum is obtained from simulations of the RSJ model. Section III clarifies the relation between the flux-noise spectrum and the complex impedance. The results from the simulations are described and discussed in Sec. IV. Particular attention is given to the implication for experimental measurements of flux noise and the complex impedance. Finally Sec. V contains some concluding remarks.

II. RSJ MODEL AND FLUX NOISE

A. RSJ model and numerical method

In our simulations we use the 2D RSJ model on a square lattice with periodic boundary conditions. This is usually assumed to be a good model of a Josephson-junction array (JJA). In particular, from the point of view of vortex fluctuations and vortex dynamics, it is expected to have the same physics as a thin superconducting film, as well as a JJA.[1] There might, however, be some differences in the level of vortex fluctuations around the transition.[13]

The RSJ model incorporates the condition of the local current conservation and the equations of motion can be written as[1]

$$\dot{\theta}_i = -\sum_j G_{ij} {\sum_k}' (\sin\phi_{jk} + \eta_{jk}), \tag{1}$$

where G_{ij} is the square lattice Green function, the primed summation is over the four nearest neighbors of the site j, and $\phi_{jk} \equiv \theta_j - \theta_k$ with the phase θ_j of the complex order parameter at site j. Here we measure time t in units of $\hbar/2eRI_c$, where R is the shunt resistance and I_c is the critical current of a single junction. The thermal noise current η_{jk} in units of I_c satisfies the conditions $\langle \eta_{ij}(t) \rangle = 0$ and

$$\langle \eta_{ij}(t)\eta_{kl}(0) \rangle = 2T(\delta_{ik}\delta_{jl} - \delta_{il}\delta_{jk})\delta(t), \tag{2}$$

where $\langle \cdots \rangle$ is the ensemble average, and the temperature T is in units of the Josephson coupling strength $J \equiv \hbar I_c/2e$.

The RSJ model may be used to calculate the current distribution in the limit of a large perpendicular penetration length $\Lambda = \Phi_0 c/4\pi^2 I_c$, where Φ_0 is the flux quantum; This is typically the case for a 2D superconductor.[1] In this limit one may replace the gauge-invariant phase difference $\phi_{jk} \equiv \theta_j - \theta_k - A_{jk}$, where $A_{jk} \equiv (2\pi/\Phi_0)\int_j^k \mathbf{A}(\mathbf{r}) \cdot d\mathbf{l}$ is the line integral of the vector potential, with $\phi_{jk} \equiv \theta_j - \theta_k$ because the coupling to the electromagnetic self-field is in this limit so weak that it has little influence on the fluctuations of the supercurrent (we are here considering the situation without an external magnetic field).[1]

We measure the flux-noise spectrum $S(\omega)$ defined by the Fourier transformation:

$$S(\omega) = \int_{-\infty}^{\infty} dt\, e^{i\omega t} S(t), \tag{3}$$

where $S(t)$ is the time-correlation function of the magnetic flux $\Phi(t)$ through a pickup coil:

$$S(t) = \langle \Phi(t)\Phi(0) \rangle \tag{4}$$

(see Sec. II B for the calculation of Φ). In addition, we calculate the dynamic dielectric function $1/\epsilon(\omega)$ of the vortices in the Coulomb-gas analogy given by[14]

$$\mathrm{Re}\left[\frac{1}{\epsilon(\omega)}\right]=\frac{1}{\epsilon(0)}+\frac{2\pi\omega T^{\mathrm{CG}}}{T^2}\int_0^\infty dt\,\sin\omega t G(t), \qquad (5)$$

$$\mathrm{Im}\left[\frac{1}{\epsilon(\omega)}\right]=-\frac{2\pi\omega T^{\mathrm{CG}}}{T^2}\int_0^\infty dt\,\cos\omega t G(t), \qquad (6)$$

where $T^{\mathrm{CG}}=T/(2\pi J\langle\cos\phi\rangle)$ is the Coulomb-gas temperature, and the time-correlation function $G(t)$ is defined by

$$G(t)\equiv\frac{1}{L^2}\langle F(t)F(0)\rangle, \qquad (7)$$

$$F(t)\equiv\sum_{\langle ij\rangle_x}\sin\phi_{ij}, \qquad (8)$$

and the sum is over all links in x direction.

The dynamic dielectric constant $1/\epsilon(\omega)$ is related to the conductivity $\sigma(\omega)$ and the complex impedance $Z(\omega)$ by[15]

$$\sigma(\omega)=Z^{-1}(\omega)=1-\frac{T}{i2\pi\omega T^{\mathrm{CG}}}\frac{1}{\epsilon(\omega)}. \qquad (9)$$

In the numerical simulation of an $L\times L$ array (in most cases $L=64$ and occasionally $L=128$ are used in the present paper), we use the periodic boundary condition for the phase variables, i.e., $\theta_{i+L\hat{\mathbf{x}}}=\theta_{i+L\hat{\mathbf{y}}}=\theta_i$, and the thermal noise currents are generated from the uniform probability distribution. For the time integration of equations of motion in Eq. (1), we use the Euler method with the discrete time step $\Delta t=0.05$. In practice we have calculated $S(t)$ up to a $t_{\max}$ beyond which $S(t)$ became so small that the simulations could not be converged well enough to obtain further information. In our simulations this turned out to be $t_{\max}\approx 100$ for $T>1.10$ and $t_{\max}\approx 400$ for lower temperatures. This means that we could not reach frequencies below $\omega\lesssim 0.016$ directly from the simulation data. However, when presenting the data we have for convenience used an extrapolation to large t based on an expected large-t behavior (this extrapolation does not change the behavior in frequency range $\omega\gtrsim 0.016$). From the ergodicity of the system, we can change the ensemble averages of the form $\langle O(t)O(0)\rangle$ in Eqs. (4) and (7) to the average $\langle O(t+t')O(t')\rangle_{t'}$ over time t', and averages over more than 10^7 time steps were typically performed.

B. Flux noise and the dipole approximation

As mentioned above, previous numerical simulations[8,9] usually calculate the noise spectra from the fluctuation of the *vorticity* defined by the directional sum of the gauge-invariant phase difference around each plaquette. The fluctuations of the total vorticity over an area of the sample is then used to estimate the flux-noise spectrum. On the other hand, in experiments[3–6] the fluctuations of the *magnetic flux* penetrating a pickup coil situated at a distance above the sample is measured. The relation between the vorticity noise and the flux noise has so far not been studied in detail and is the subject of the present paper.

We consider three distinct cases: The first one is the fluctuation of the magnetic flux associated with the vortices on a fixed area A of the sample. The vortices describe the rotation of the supercurrent on the sample.[1] This means that the magnetic flux associated with an elementary plaquette is proportional to the rotation of the supercurrent around the plaquette. For the RSJ model the magnetic flux for a plaquette is then given by[7,14,16]

$$n(\mathbf{r})\equiv\frac{T^{\mathrm{CG}}}{T}\sum_p \sin\phi_{ij}, \qquad (10)$$

in units of the flux quantum ϕ_0.[17] Here $\mathbf{r}$ is the central position of the plaquette and the summation is around the plaquette p. Consequently the total magnetic flux associated with the rotation of the supercurrent at a given time t is

$$\Phi(t)=\int_A d^2r\, n(\mathbf{r},t),$$

where the integral over position denotes the sum over all elementary squares inside the area A.

The second case is the fluctuation of the vorticity associated with a fixed area A of the sample. The vorticity of an elementary plaquette is given by[1]

$$v(\mathbf{r})\equiv\frac{1}{2\pi}\sum_p \phi_{ij}, \qquad (11)$$

where the phase difference ϕ_{ij} is restricted to the interval $-\pi<\phi_{ij}\leqslant\pi$. The total vorticity $V(t)$ associated with the area A is consequently

$$V(t)=\int_A d^2r\, v(\mathbf{r},t).$$

The third case corresponds to the experimental situation where one measures the magnetic flux through a pickup coil situated a distance d from the sample. Note that the first case corresponds to the case when $d=0$. However, in typical experiments d is a macroscopic length (typically of the order of 0.1 mm).[4–6]

In this section, we focus on the third case and use a dipole approximation to obtain an expression for the magnetic flux through a pickup coil at a distance d from the sample where $d\gg\Lambda$. At this distance the magnetic-field distribution from a vortex is of dipole form. In the continuum limit only the circulation of the supercurrent around a closed loop which encloses a vortex core region gives a finite value. This value can be positive or negative but has the same magnitude for all closed loops which enclose vortex cores.[1] This means that one can estimate the magnetic field at $d\gg\Lambda$ from the circulation of the supercurrent around small closed loops which cover the area of the superconductor by associating each of these loops with a dipole field where the strength of the dipole moment is proportional to the circulation of the supercurrent. This approximation is readily carried over to the array. The circulation of the supercurrent around a plaquette in units of I_c is given by [see Fig. 1(a)][18]

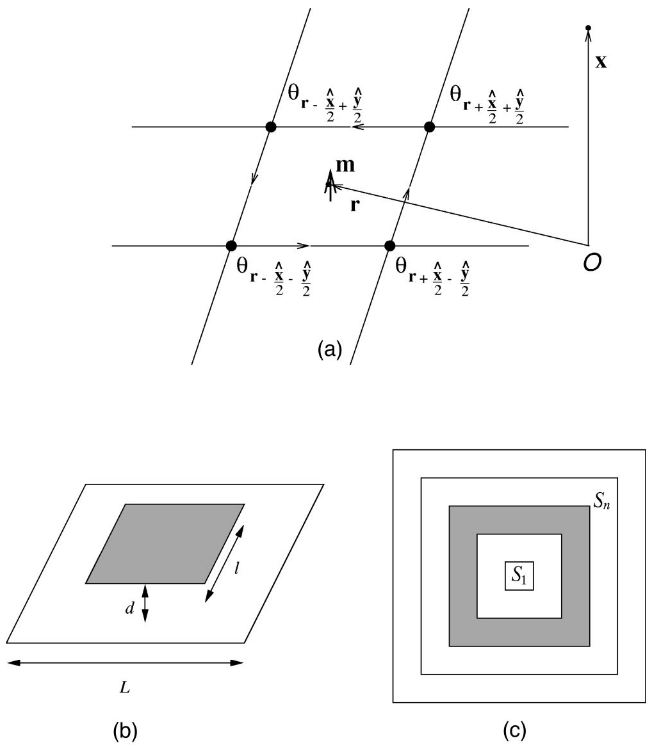

FIG. 1. (a) The vortex dipole moment associated with the dual lattice point $\mathbf{r}$ is estimated by the circulating current around the plaquette. The magnetic field at the observation point $\mathbf{x}$ is the summation of the contributions from all such vortex dipole moments. (b) The $l\times l$ pickup coil is separated by the distance d from the $L\times L$ square array of Josephson junctions. (c) The whole array is divided into quadratic enclosures. The plaquettes surrounding such an enclosure is denoted by S_n (shaded area). The magnetic flux due the plaquettes belonging to S_n is calculated.

$$\begin{aligned}\sin\left[\phi\left(\mathbf{r}-\frac{\hat{\mathbf{x}}}{2}-\frac{\hat{\mathbf{y}}}{2},\mathbf{r}+\frac{\hat{\mathbf{x}}}{2}-\frac{\hat{\mathbf{y}}}{2}\right)\right]&\\ +\sin\left[\phi\left(\mathbf{r}+\frac{\hat{\mathbf{x}}}{2}-\frac{\hat{\mathbf{y}}}{2},\mathbf{r}+\frac{\hat{\mathbf{x}}}{2}+\frac{\hat{\mathbf{y}}}{2}\right)\right]&\\ +\sin\left[\phi\left(\mathbf{r}+\frac{\hat{\mathbf{x}}}{2}+\frac{\hat{\mathbf{y}}}{2},\mathbf{r}-\frac{\hat{\mathbf{x}}}{2}+\frac{\hat{\mathbf{y}}}{2}\right)\right]&\\ +\sin\left[\phi\left(\mathbf{r}-\frac{\hat{\mathbf{x}}}{2}+\frac{\hat{\mathbf{y}}}{2},\mathbf{r}-\frac{\hat{\mathbf{x}}}{2}-\frac{\hat{\mathbf{y}}}{2}\right)\right],&\qquad(12)\end{aligned}$$

where $\phi(\mathbf{r}',\mathbf{r}'')\equiv\theta_{\mathbf{r}'}-\theta_{\mathbf{r}''}$ and $\theta_{\mathbf{r}'}$ is the phase of the complex order parameter at site $\mathbf{r}'$. The contribution to the magnetic field at large distances from this circulation can then approximately be described in terms of a dipole moment $\mathbf{m}_{\mathbf{r}}=m_{\mathbf{r}}\hat{\mathbf{z}}$ proportional to the circulation. The magnetic field at the observation point $\mathbf{x}$ due to this vortex dipole moment $\mathbf{m}_{\mathbf{r}}$ is given by[19]

$$\mathbf{B}(\mathbf{x})=\sum_{\mathbf{r}}\frac{3\mathbf{e}_{\mathbf{rx}}(\mathbf{e}_{\mathbf{rx}}\cdot\mathbf{m}_{\mathbf{r}})-\mathbf{m}_{\mathbf{r}}}{|\mathbf{x}-\mathbf{r}|^3},\qquad(13)$$

where $\mathbf{e}_{\mathbf{rx}}\equiv(\mathbf{x}-\mathbf{r})/|\mathbf{x}-\mathbf{r}|$ is the unit vector in the direction of $\mathbf{x}-\mathbf{r}$ and the summation is over all dual lattice points (central positions of plaquettes). The magnetic flux through the pickup coil [the shaded area in Fig. 1(b)] separated by distance d from the array is given by the surface integral:

$$\Phi=\int_{\mathrm{coil}}\mathbf{B}(\mathbf{x})\cdot d\mathbf{s}.\qquad(14)$$

We consider the case $d\gg a$ so that the magnetic field inside the pickup coil does not vary much on a microscopic length scale a. We may then replace the integral Eq. (14) by the discrete summation:

$$\begin{aligned}\Phi&\approx\sum_{\mathbf{r}'\in l\times l}\mathbf{B}(\mathbf{r}'+d\hat{\mathbf{z}})\cdot\hat{\mathbf{z}}\\ &=\sum_{\mathbf{r}'\in l\times l}\sum_{\mathbf{r}\in L\times L}\frac{3\mathbf{n}_{\mathbf{rr}'}(\mathbf{n}_{\mathbf{rr}'}\cdot\mathbf{m}_{\mathbf{r}})-\mathbf{m}_{\mathbf{r}}}{|\mathbf{r}'+d\hat{\mathbf{z}}-\mathbf{r}|^3}\cdot\hat{\mathbf{z}}\\ &=\sum_{\mathbf{r}'\in l\times l}\sum_{\mathbf{r}\in L\times L}\frac{3d^2-|\mathbf{r}'+d\hat{\mathbf{z}}-\mathbf{r}|^2}{|\mathbf{r}'+d\hat{\mathbf{z}}-\mathbf{r}|^5}m_{\mathbf{r}},\end{aligned}\qquad(15)$$

where $\mathbf{x}$ is decomposed into $\mathbf{x}=\mathbf{r}'+d\hat{\mathbf{z}}$, and the two 2D vectors $\mathbf{r}$ and $\mathbf{r}'$ denote positions on the array. The summations $\Sigma_{\mathbf{r}'}$ and $\Sigma_{\mathbf{r}}$ are performed on the $l\times l$ pickup coil and the $L\times L$ whole array, respectively [see Fig. 1(b)]. Since Eq. (15) contains $O(L^4)$ terms (in this work we choose $l=L/2$), the calculation of the magnetic flux in this way requires most of the computer time in the numerical simulations. This time-consuming part is avoided in the approximate scheme we use in our simulation to obtain the results described in Sec. IV.

We use the following approximate scheme: The whole array is divided into stripes formed by elementary plaquettes which enclose the midpoint of the pickup coil as the sides of a square. This is illustrated in Fig. 1(c). Each such collection of elementary plaquettes are denoted by S_n where $2n-1$ is the number of plaquettes of each of the four stripes forming the sides of the square. The magnetic flux in Eq. (15) is expressed as the summation of the contributions from each S_n:

$$\Phi=\sum_n q_nM_n,\qquad(16)$$

where M_n is the summation of the vortex dipole moments for the plaquettes forming S_n and q_n is the appropriate weight factor:

$$q_n\equiv\left(\sum_{\mathbf{r}\in S_n}m_{\mathbf{r}}\sum_{\mathbf{r}'\in l\times l}\frac{3d^2-|\mathbf{r}'+d\hat{\mathbf{z}}-\mathbf{r}|^2}{|\mathbf{r}'+d\hat{\mathbf{z}}-\mathbf{r}|^5}\right)\left(\frac{1}{\sum_{\mathbf{r}\in S_n}m_{\mathbf{r}}}\right),\qquad(17)$$

$$M_n\equiv\sum_{\mathbf{r}\in S_n}m_{\mathbf{r}}.\qquad(18)$$

We now assume that $m_{\mathbf{r}}$ in Eq. (17) can to good approximation be replaced by the average value for each S_n, i.e., $\tilde{m}_{\mathbf{r}}=\Sigma\mathbf{r}\in S_nm_{\mathbf{r}}/A_n$ where A_n is the number of plaquettes contained in S_n. This simplifies Eq. (17) to

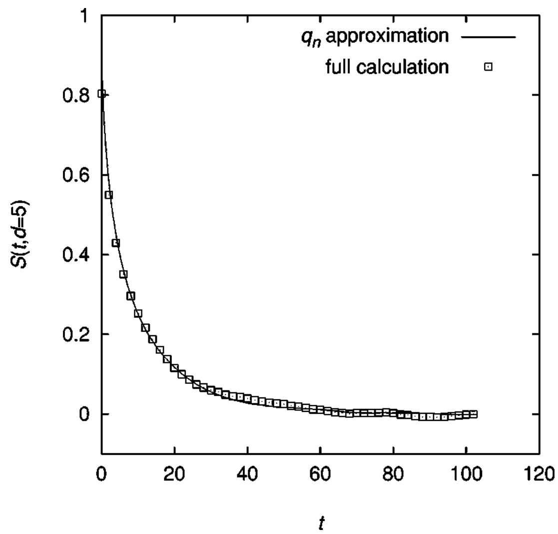

FIG. 2. Comparison between the flux noise from the full calculation [Eq. (15)] and from the approximate scheme [Eqs. (16), (18), and (19)]. The figure shows the flux noise as a function of time t, $S(t,d) \equiv \langle \Phi(t,d)\Phi(0,d)\rangle$ for a 16×16 coil with the distance $d=5$ from a 32×32 array at the temperature $T=1.10$ (in units of J/k_B). As seen the approximation scheme reproduces the full calculation very accurately.

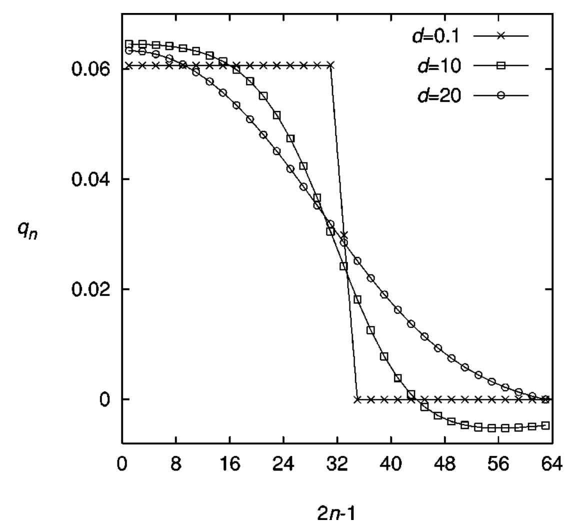

FIG. 3. The weight factor q_n (in arbitrary unit) for S_n plotted against the size $2n-1$ (in numbers of plaquettes per side). The data are for a 64×64 array with the coil size 32×32 for different distances d. When the distance d between the coil and the array is very small, only plaquettes inside of the pickup coil contribute to the magnetic flux, whereas all plaquettes contribute for larger d.

$$q_n = \frac{1}{A_n}\sum_{\mathbf{r}\in S_n}\sum_{\mathbf{r}'\in l\times l}\frac{3d^2-|\mathbf{r}'+d\hat{\mathbf{z}}-\mathbf{r}|^2}{|\mathbf{r}'+d\hat{\mathbf{z}}-\mathbf{r}|^5}. \tag{19}$$

The magnetic flux in Eq. (16) can by aid of Eqs. (18) and (19) be computed in $O(L^2)$ operations, since q_n within this approximation is a purely geometric quantity which is independent of time. In Fig. 2 we compare the flux noise $S(t,d)\equiv\langle\Phi(t,d)\Phi(0,d)\rangle$ from the full calculation in Eq. (15) and the q_n approximation in Eqs. (16) and (19) for a 32×32 array with a 16×16 coil size and the distance $d=5$. It is clearly shown that the approximation made in Eq. (19) is indeed a very good approximation.

Figure 3 shows q_n as a function of the linear size $(2n-1)$ of S_n for $d=0.1$, 10, and 20 (a 32×32 pickup coil is used for a 64×64 array). For very small values of d, q_n becomes a step function where only S_n's inside the pickup coil contribute to the magnetic flux. On the other hand, as d is increased, it is clearly seen that there is a significant contribution to the magnetic field caused by the S_n's outside the pickup coil area. In previous numerical studies of the flux-noise spectra the magnetic flux has usually been approximated by the vorticity inside the pickup coil area (the second case mentioned in the beginning of this subsection).[8,9] This approximation hence does not take the contributions from S_n's outside the pick-up coil area into account and in this sense it corresponds to $d=0$. One conclusion from the present work is that for a more precise comparison with experiments one should instead consider the opposite case of large d. The results of our simulations are presented in Sec. IV. In the following section we elucidate the relation between the flux-noise spectrum and the complex impedance, or equivalently the complex conductivity.

III. FLUX NOISE AND CONDUCTIVITY

In this section we consider for simplicity a 2D superconductor in the continuum limit so that, compared to the previous section, the limit $a\rightarrow 0$ is implied instead of $a=1$. The magnetic flux associated with the area d^2r around $\mathbf{r}$ is then $n(\mathbf{r})d^2r$ [see Eq. (10)]. In the Coulomb-gas analogy of vortices, $n(\mathbf{r})$ is the charge-density.[1,14,16] The charge-density correlation function is given by $c(r,t)=\langle n(r,t)n(0,0)\rangle$. We will first relate $c(r,t)$ to the dielectric function $1/\hat{\epsilon}(\mathbf{k},\omega)$ and the conductivity $\sigma(\omega)$ of the superconductor: The charge-density correlation function $c(r,t)$ is related to the charge-density response function $g(r,t)$ by

$$\mathrm{Im}[\hat{g}(\mathbf{k},\omega)] = \frac{\omega}{2T^{\mathrm{CG}}}\hat{c}(\mathbf{k},\omega), \tag{20}$$

where $\hat{g}$ and $\hat{c}$ denote the Fourier transforms. The dielectric function $1/\hat{\epsilon}(\mathbf{k},\omega)$ is given by the usual linear-response relation[1]

$$\frac{1}{\hat{\epsilon}(\mathbf{k},\omega)} = 1-\frac{2\pi}{k^2}\hat{g}(\mathbf{k},\omega). \tag{21}$$

We define $1/\epsilon(\omega)\equiv 1/\hat{\epsilon}(\mathbf{k}=0,\omega)$ which means that Eqs. (20) and (21) for $\mathbf{k}=0$ corresponds to Eqs. (5) and (6) for the RSJ model. From Eqs. (9), (20), and (21) we obtain a relation between the charge-density correlations $c(r,t)$ and the real part of the conductivity $\sigma(\omega)$:

$$\mathrm{Re}[\sigma(\omega)] = -\frac{T}{2\pi T^{\mathrm{CG}}\omega}\mathrm{Im}\left[\frac{1}{\epsilon(\omega)}\right], \tag{22}$$

and

$$\mathrm{Im}\left[\frac{1}{\epsilon(\omega)}\right] = -\frac{\pi\omega}{T^{\mathrm{CG}}}\lim_{k\rightarrow 0}\frac{\hat{c}(k,\omega)}{k^2}. \tag{23}$$

Next we relate the charge-density correlation function $c(r,t)$ to the flux-noise spectrum. From Eq. (15) we have that the magnetic flux measured by the pickup coil is

$$\Phi = \int_{\text{coil}} B_z(\mathbf{r}) d^2 r,$$

where the integral is over the area covered by the coil. The magnetic field $B_z(\mathbf{r})$ can be expressed as

$$B_z(\mathbf{r}) = \int f(|\mathbf{r}'-\mathbf{r}|,d) n(\mathbf{r}) d^2 r',$$

the r' integration is over the whole 2D plane, and from Eqs. (10) and (15), we have

$$f(r,d) = \frac{T}{T^{\text{CG}}} \frac{3d^2-(r^2+d^2)}{(r^2+d^2)^{5/2}}. \tag{24}$$

This means that the flux-noise spectrum $S(t) = \langle \Phi(t)\Phi(0)\rangle$ is given by

$$S(t) = \int_{\text{coil}} d^2 r \int_{\text{coil}} d^2 r' \int d^2 r'' \int d^2 r''' f(|\mathbf{r}''-\mathbf{r}|,d) \times \langle n(\mathbf{r},t) n(\mathbf{r}',0)\rangle f(|\mathbf{r}'-\mathbf{r}'''|,d). \tag{25}$$

We can now use the convolution theorem and express $S(t)$ in terms of the Fourier transforms of $f(r,d)$ and $c(r,t) = \langle n(r,t) n(0,0)\rangle$, i.e.,

$$S(t) = \int_{\text{coil}} d^2 r \int_{\text{coil}} d^2 r' \int \frac{d^2 k}{(2\pi)^2} e^{i\mathbf{k}\cdot(\mathbf{r}-\mathbf{r}')} |\hat{f}(k,d)|^2 \hat{c}(k,t).$$

Taking the Fourier transform of $S(t)$ and using the connection between $\hat{c}(k,\omega)$ and $1/\hat{\epsilon}(\mathbf{k},\omega)$ given by Eqs. (20) and (21) yields

$$S(\omega) = -\int_0^\infty dk\, \hat{F}(k,d) \text{Im}\left[\frac{1}{\hat{\epsilon}(k,\omega)}\right], \tag{26}$$

where

$$\hat{F}(k,d) = \frac{2T^{\text{CG}}}{(2\pi)^2 \omega} \int_{\text{coil}} d^2 r \int_{\text{coil}} d^2 r' e^{i\mathbf{k}\cdot(\mathbf{r}-\mathbf{r}')} k^3 |\hat{f}(k,d)|^2, \tag{27}$$

and $\hat{f}(k,d)$ is the Fourier transform of $f(r,d)$ which describes the spreading of the magnetic field. Within the dipole approximation of Eq. (24) $\hat{f}(k,d)$ is given by

$$\hat{f}(k,d) = \frac{T}{T^{\text{CG}}} 2\pi k e^{-kd}. \tag{28}$$

The extreme case $d=0$ is outside the dipole approximation and is given by

$$\hat{f}(k) = \frac{T}{T^{\text{CG}}}. \tag{29}$$

The important point to note is that the flux-noise spectrum $S(\omega)$ is directly related to the response function $\text{Im}[1/\hat{\epsilon}(k,\omega)]$ through a function $\hat{F}(k,d)$ which contains all the information of the spreading of the magnetic field above the superconductor as well as the geometry and position of the pickup coil.

In Ref. 7 it was suggested that the relation between the flux noise $S(\omega)$ and $\text{Im}[1/\hat{\epsilon}(k,\omega)]$ could be further simplified to

$$S(\omega) \propto \frac{1}{\omega} \left| \text{Im}\left[\frac{1}{\hat{\epsilon}(0,\omega)}\right] \right|,$$

or equivalently

$$S(\omega) \propto \text{Re}[\sigma(\omega)]. \tag{30}$$

We will here show that for the typically experimental situation this proportionality between the conductivity and the flux noise is indeed valid.

In order to establish this we assume for simplicity that the pickup coil is circular with radius R. In this case it is possible to obtain an explicit expression for $\hat{F}(k,d)$ in Eq. (27), i.e.,

$$\hat{F}(k,d) = \frac{2T^{\text{CG}}}{\omega} R^2 k |\hat{f}(k,d)|^2 [J_1(kR)]^2, \tag{31}$$

where J_1 is the Bessel function of order one. Let us first consider the limit in which the dipole approximation Eq. (24) is valid. This limit implies that the distance d to the pickup coil is sufficiently large compared to the relevant microscopic lengths. For a Josephson-junction array the microscopic length is the lattice constant a which is typically of the order 1–10 μm whereas for a continuum superconductor it is the size of a vortex core typically given by the Ginzburg-Landau coherence length ξ and is of the order of 100–1000 Å close to the transition. In addition, Λ has to be much larger than a for a Josephson-junction array and ξ for a superconducting film. The typical size of d is 100 μm.[3–6] So in practice the vortex dipole approximation may be expected to be valid for superconducting films but the validity for Josephson-junction arrays may be more questionable. When the vortex dipole approximation is valid the noise spectrum is given by [compare Eqs. (26), (28), and (31)]

$$S_R(\omega) = -\frac{8\pi^2 T^2 R^2}{T^{\text{CG}}\omega} \int_0^\infty dk\, k^3 e^{-2kd} [J_1(kR)]^2 \text{Im}\left[\frac{1}{\hat{\epsilon}(k,\omega)}\right]. \tag{32}$$

One notes that k values much larger than $1/d$ will not contribute to the integral in Eq. (32) because of the factor e^{-2kd}. This means that if d is sufficiently large compared to the relevant microscopic length, then $\text{Im}[1/\hat{\epsilon}(k,\omega)]$ can be replaced by $\text{Im}[1/\hat{\epsilon}(0,\omega)]$, demonstrating that under these conditions $S(\omega)$ is indeed proportional to $\text{Im}[1/\omega\hat{\epsilon}(0,\omega)]$. In the present case of a circular pickup coil we explicitly find

$$S_R(\omega) = -\frac{C}{\omega} \text{Im}\left[\frac{1}{\hat{\epsilon}(0,\omega)}\right],$$

where the proportionality constant C is given by (after changing the integration variable to $x = kd$)

$$C=\frac{8\pi^2T^2}{T^{\mathrm{CG}}}\frac{R^2}{d^4}\int_0^\infty dx\, x^3e^{-2x}[J_1(xR/d)]^2.$$

In the limit $R/d \ll 1$ this reduces to

$$C\approx\frac{T^2}{T^{\mathrm{CG}}}\frac{R^4}{d^6}\frac{15\pi^2}{4}, \tag{33}$$

and in the limit $R/d \gg 1$ to

$$C\approx\frac{T^2}{T^{\mathrm{CG}}}\frac{2\pi R}{d^3}. \tag{34}$$

We conclude from Eqs. (33) and (34) that the proportionality constant C will always contain a temperature-dependent factor T^2/T^{CG} and a dependence on the size of the coil. This coil-size dependence reflects the relative magnitudes between the coil size and the distance from the sample: When R is much larger than d, the noise amplitude is proportional to the perimeter of the coil $2\pi R$, and, when it is much smaller, it is proportional to square of the coil area R^4. In typical experiments R is usually much larger than d.[3–6]

In some previous simulations of the flux-noise spectrum, based on the XY models, one has approximated the flux-noise spectrum from the fluctuation of the total vorticity for a finite area of the model.[8,9] This implies two differences in relation to the above dipole approximation: First of all it corresponds to $d=0$ and consequently to a constant $\hat{f}$ [see Eq. (29)]. Secondly, it corresponds to changing the magnetic flux defined by Eq. (10) to vorticity defined by Eq. (11). Let us first consider the first change by itself: The case of a circular area with radius R then corresponds to the flux noise [compare Eqs. (26), (29), and (31)]

$$S_R(\omega)=-\frac{2T^2}{\omega T^{\mathrm{CG}}}R^2\int_0^\infty dk\, k[J_1(kR)]^2\,\mathrm{Im}\left[\frac{1}{\hat{\epsilon}(k,\omega)}\right]. \tag{35}$$

This means that, in this case, the flux-noise spectrum depends on all the k values of $\mathrm{Im}[1/\hat{\epsilon}(k,\omega)]$ and is not proportional to $\mathrm{Im}[1/\hat{\epsilon}(0,\omega)]$. For example the leading large-R dependence of Eq. (35) is

$$S_R(\omega)\propto-\frac{R}{\omega}\int_0^\infty dk\,\mathrm{Im}\left[\frac{1}{\hat{\epsilon}(k,\omega)}\right].$$

So in this limit the flux noise is proportional to the perimeter of the pickup area just as for the large-d case, but instead of singling out the $k=0$ contribution all k values contribute. The proportionality between the flux noise $S(\omega)$ and $\mathrm{Im}[1/\omega\hat{\epsilon}(0,\omega)]\propto\mathrm{Re}[\sigma(\omega)]$ can be tested by experiments since both $S(\omega)$ and the conductivity $\sigma(\omega)$ can be independently measured.[6]

The change from magnetic flux [defined by Eq. (10)] to vorticity [defined by Eq. (11)] influences the flux-noise spectrum in an additional significant way: Now the crossing of a vortex over the perimeter of the pickup area is described as a discrete $\pm 2\pi$ change of the total vorticity of the pick-up area. The corresponding spectrum hence corresponds to a random walk of discrete events over a sharp boundary. This results in a $\omega^{-3/2}$ tail of the spectrum.[20] However, this condition does not correspond to the experimental situation where the pickup coil does not have a sharp boundary, is at a distance d from the sample, and, most importantly, the magnetic field from a vortex is spread out. In the next section we present numerical results of the flux-noise spectrum and its relation to the conductivity.

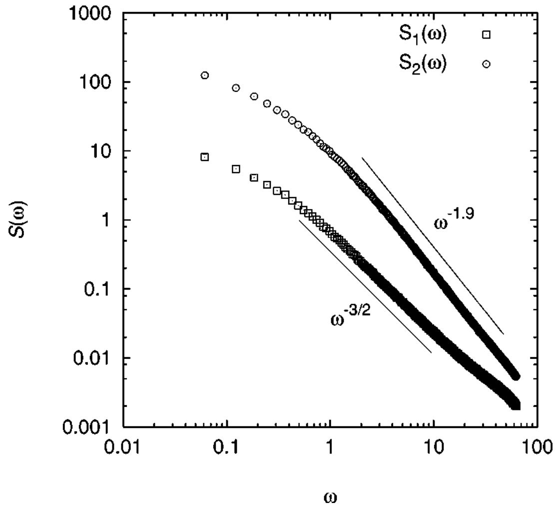

FIG. 4. Comparison between the vorticity-noise spectrum S_1 and the magnetic-flux-noise spectrum S_2 for $d=0$. The data are for a 64×64 array at $T=1.1$ with a 32×32 coil size. The vorticity spectrum has a $\omega^{-3/2}$ tail, whereas the magnetic-flux spectrum is closer to ω^{-2} (Ref. 21).

IV. SIMULATION RESULTS AND EXPERIMENTAL IMPLICATIONS

A. Comparison with previous works

We first relate our simulations results to earlier ones for the RSJ model.[8,9] These earlier simulations calculated the noise spectrum of the *vorticity* [see Eq. (11)] over a fixed area of the systems (the $d=0$ case).[8,9] As explained in the previous section, this corresponds to discrete events over a sharp boundary and implying a $\omega^{-3/2}$-tail.[20] Such a tail has indeed been found in Ref. 8 and is also verified in our simulations.[21] This is apparent from Fig. 4 which displays our data for a 64×64 array with a pickup area of size 32×32 at $T=1.1$; the lower data set shows the *vorticity*-noise spectrum and the slope is $-3/2$. However, if we instead calculate the *magnetic-flux*-noise spectrum [see Eq. (10)], then the crossing of magnetic flux over the perimeter is not a discrete event. This means that there is no obvious reason for a $\omega^{-3/2}$ tail and nor do we find any such tail in the simulations, as is also apparent from Fig. 4. The exponent in Fig. 4 for this case is instead close to -2 as seen from the upper data set in Fig. 4.[22]

B. Flux-noise spectra with a finite distance between pickup coil and array

As mentioned in Sec. III the typical experimental setup measures the *magnetic-flux*-noise spectrum with a finite distance d between the array and the pickup coil.[3–6] Furthermore, the typical experimental setup corresponds to the

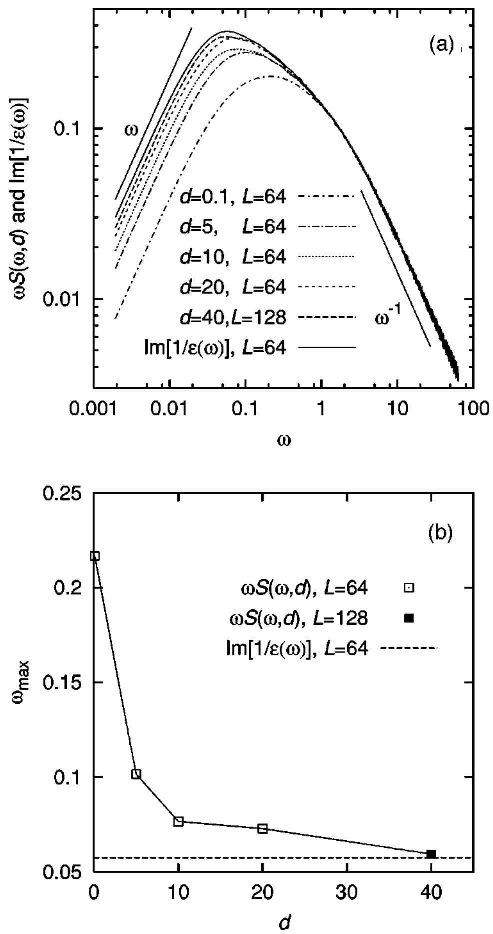

FIG. 5. (a) The dependence of the flux-noise spectrum $S(\omega,d)$ on the distance d. The full drawn uppermost curve is the imaginary part of the dielectric function $|\mathrm{Im}[1/\epsilon(\omega)]|$. The rest of the curves correspond to $d=0.1$, 5, 10, 20, and 40 (from bottom to top) plotted as $\omega S(\omega,d)$ and the curves are shifted in the vertical direction for better comparison. The data are for a 64×64 array with a 32×32 pick-up coil at $T=1.1$, except for $d=40$ where a 128×128 array was necessary because plaquettes further away from the center contribute in this case. As d is increased $\omega S(\omega,d)$ approaches $|\mathrm{Im}[1/\epsilon(\omega)]|$. (b) The frequency at the maxima for the curves in (a) are plotted versus the distance d. As d is increased, this frequency decreases and approaches the value for $|\mathrm{Im}(1/\epsilon(\omega)|$. (The full line is a guide to the eye.)

large-d limit where the noise spectrum $S(\omega)$ is proportional to the real part of the conductivity $\sigma(\omega)$ (see Sec. III).

In our simulations we investigate the flux-noise spectra as a function of the distance d to the pickup coil. Figure 5(a) shows the flux-noise spectra calculated from Eqs. (3) and (4) with the magnetic flux given by Eqs. (16), (18), and (19) (see Sec. II B for details). The data sets are shown as $\omega S(\omega,d)$ against ω in a log-log plot. The vertical scale is adjusted in order to compare the shapes of the curves. One notices that the spectra for the different d's all approach ω^{-1} for large ω and can be collapsed to a single curve in this large-ω region by a vertical adjustment. For small ω the curves become linear with ω which reflects a constant part (white noise) of $S(\omega,d)$.[5,6,8,9] As d increases the peak of the $\omega S(\omega,d)$ curves moves to the left and the peak height increases. The uppermost curve in Fig. 5(a) is $|\mathrm{Im}[1/\epsilon(\omega)]|$ (full curve in the figure) and, as d is increased, the flux-noise spectrum $\omega S(\omega,d)$ approaches this uppermost curve. This verifies that for large d one has the simple connection $S(\omega) \propto |\mathrm{Im}[1/\omega\epsilon(\omega)]|$ as discussed in Sec. III.

Figure 5(b) shows that the characteristic frequency given by the peak position in Fig. 5(a) decreases with increasing d. In the limit of large d the characteristic frequency of $S(\omega,d)$ agrees with the characteristic frequency of $1/\epsilon(\omega)$. Thus in this limit both the shape and the characteristic frequency of $S(\omega,d)$ and $\mathrm{Im}[1/\omega\epsilon(\omega)]$ are the same. This proportionality between the flux-noise spectrum and complex conductivity can be tested experimentally and indeed seems to be borne out.[6]

The fact that the flux-noise spectrum in the large-d limit is proportional to real part of the conductivity means that the characteristic features of the conductivity are reflected in the flux-noise spectrum. In case of a 2D superconductor the dynamical features of the conductivity $\sigma(\omega)\propto -1/i\omega\epsilon(\omega)$, are well described by the response form[14]

$$\mathrm{Re}\left[\frac{1}{\epsilon(\omega)}\right]-\frac{1}{\epsilon(0)}=\frac{1}{\tilde{\epsilon}}\frac{\omega}{\omega+\omega_0}, \tag{36}$$

and

$$\mathrm{Im}\left[\frac{1}{\epsilon(\omega)}\right]=-\frac{1}{\tilde{\epsilon}}\frac{2}{\pi}\frac{\omega\omega_0\ln\omega/\omega_0}{\omega^2-\omega_0^2}, \tag{37}$$

which catches the dynamics of vortex fluctuations in a region around the KT transition. From Eq. (37) one notices that the peak of $|\mathrm{Im}[1/\epsilon(\omega)]|$ occurs at the characteristic frequency ω_0 and that the peak height is $1/\pi\tilde{\epsilon}$. Above the KT transition $1/\tilde{\epsilon}$ increases only weakly with increasing temperature and approaches unity for somewhat higher temperatures.[14] For the flux-noise spectrum this means that $S(\omega_0)\propto T^2/T^{\mathrm{CG}}\tilde{\epsilon}\omega_0$. Now $T/T^{\mathrm{CG}}\propto\rho_0(T)$ where $\rho_0(T)$ is the bare superfluid density which decreases slightly with temperature[1] whereas T increases so that also T^2/T^{CG} depends only weakly on T. This means that to good approximation the flux-noise spectrum for different temperatures above the KT transition should have a common tangent$\propto 1/\omega$ which goes through all the points $S(\omega_0(T),T)$. This means that the common tangent in a log-log plot has the slope -1. This feature is illustrated in Fig. 6 which demonstrates the existence of a common tangent with the slope close to -1 both directly for $S(\omega,d)$ and for $\mathrm{Re}[\sigma(\omega)]\propto -\mathrm{Im}[1/\omega\epsilon(\omega)]$. The existence of a common tangent for the flux-noise spectra with the slope -1 can be readily tested in experiments and seems to be well borne out.[6,23]

One should, however, notice that the argument for a common tangent with slope -1 does not single out the response form given by Eqs. (36) and (37). In fact, the reasoning is also valid in a region above the KT transition where the response of the vortex fluctuations is given by the conventional Drude response form

$$\mathrm{Re}\left[\frac{1}{\epsilon(\omega)}\right]=\frac{1}{\tilde{\epsilon}}\frac{\omega^2}{\omega^2+\omega_0^2}, \tag{38}$$

and

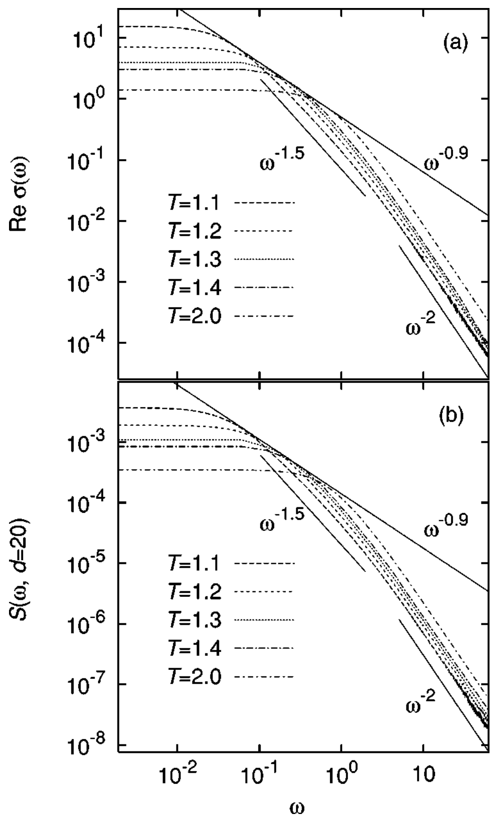

FIG. 6. (a) The real part of the conductivity $\mathrm{Re}[\sigma(\omega)]$ and (b) the flux-noise spectrum $S(\omega,d=20)$ at temperatures above the KT transition. The curves for $\mathrm{Re}[\sigma(\omega)]$ and $S(\omega,d=20)$ have the same shape; for small frequencies they have a very weak ω dependence, for somewhat larger ω there is an approximate $\omega^{-3/2}$-behavior, whereas for even larger ω the behavior approaches ω^{-2}. The curves in the log-log plot have a common tangent with the slope -0.9.

$$\mathrm{Im}\left[\frac{1}{\epsilon(\omega)}\right]=-\frac{1}{\tilde{\epsilon}}\frac{\omega\omega_0}{\omega^2+\omega_0^2}. \tag{39}$$

which gives the peak height $1/2\tilde{\epsilon}$. One expects that the response form Eqs. (36) and (37) describes the response from the vortex pairs in a region just above the KT transition whereas the conventional Drude response is obtained for higher temperatures where the response is dominated by free vortices.[14] How wide these regions are depend on the details: for a real thin superconductor the vortex-pair-response seems to dominate in a wide region.[14] However, for the 2D RSJ model on a square lattice, which we are using here, the vortex-pair-dominated region above the KT transition is narrow and the Drude response dominates in a broader region above the KT transition. Thus, the data shown in Fig. 6 are predominantly Drude-like. A practical way of determining which response type is at hand is to measure the complex impedance and determine the peak ratio [i.e., the ratio $\mathrm{Re}(\sigma)/\mathrm{Im}(\sigma)$ at the peak position ω_0 of $\mathrm{Re}(\sigma/\omega)$]; for the vortex-pair-dominated response, Eqs. (36) and (37), this ratio is $2/\pi\approx 0.64$ and for free vortex Drude response, Eqs. (38) and (39), it is unity.[14]

The essential point here is that, because the flux-noise spectrum for a large d is proportional to $\mathrm{Re}[\sigma(\omega)]$, the noise spectra at a sequence of temperatures above the KT transition should in a log-log plot have a common tangent with slope -1. We can substantiate this claim further by simulating the noise spectra for a small d where the flux-noise spectrum is *not* proportional to $\mathrm{Re}[\sigma(\omega)]$. In this case there is no particular reason for a common tangent with any slope and, as apparent from the simulation results in Fig. 7, no such common tangent can be fitted to the data.

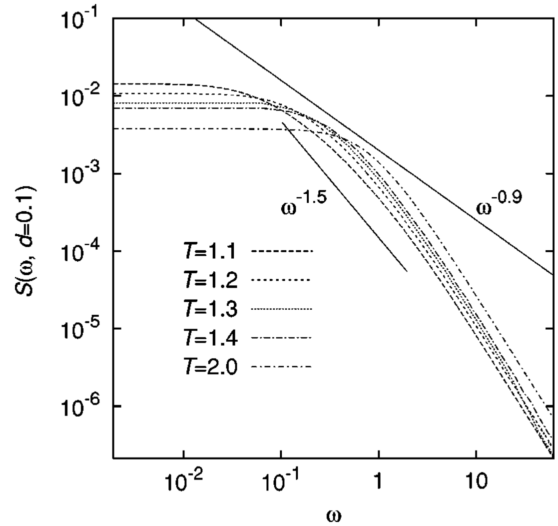

FIG. 7. Flux-noise spectrum in the small-d limit at temperatures above the KT transition [same as Fig. 6(b) but with $d=0.1$ instead of $d=20$]. In the case of small d we find neither a common tangent nor an appreciable range of $\omega^{-1.5}$ behavior.

One may also notice from Fig. 6 that both $S(\omega,d)$ and $\mathrm{Re}[\sigma(\omega)]$ have intermediate regions with $\omega^{-1.5}$ followed by a ω^{-2} tail for even larger ω. However, such an intermediate-$\omega^{-1.5}$ region appears to be less discernible for the small-d case when $S(\omega,d)$ is not proportional to $\mathrm{Re}[\sigma(\omega)]$, as is apparent from Fig. 7.

C. Flux-noise spectrum below KT transition

Next we investigate what happens as the temperature is decreased towards the KT transition and below. Figure 8 shows data for $\mathrm{Im}[1/\epsilon(\omega)]$ and $\omega S(\omega,d=20)$ over a wider range of temperatures (the data for $T\geqslant 1.1$ are the same as in Fig. 6). Again one observes that both quantities behave in precisely the same way over the whole temperature range, verifying that they are indeed proportional to very good approximation. Next one observes that the characteristic frequency ω_0 (the frequency of the peak position) decreases as the KT transition is approached from above. This suggests a critical slowing down at the KT transition to $\omega_0=0$.[8,14] As the temperature passes through the transition the characteristic frequency starts to increase again (the full curves in Fig. 8 are below the KT transition).[8,14]

The argument for a common $1/\omega$ tangent for the flux-noise spectra above the KT transition is related to the fact that the peak height for $|\mathrm{Im}[1/\epsilon(\omega)]|$ is $1/\pi\tilde{\epsilon}$ $(1/2\tilde{\epsilon})$ for the vortex pair response, Eqs. (36) and (37) [free vortex Drude response, Eqs. (38) and (39)] together with the fact that $1/\tilde{\epsilon}$ only increases very weakly with T above the KT transition and approaches unity for somewhat higher T. Figure 8 shows

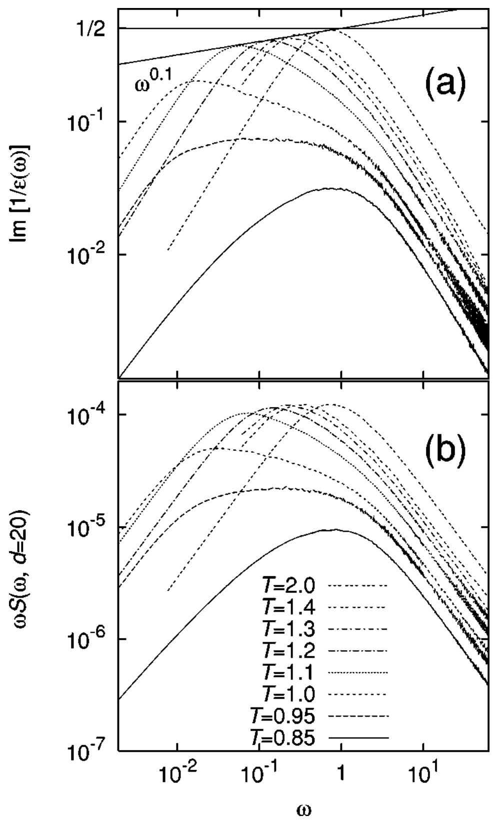

FIG. 8. (a) The imaginary part of the dielectric function, $|\mathrm{Im}[1/\epsilon(\omega)]|$, and (b) the flux-noise spectrum multiplied by the frequency, $\omega S(\omega,d=20)$, at temperatures above and below the KT transition. This again illustrates that both quantities behave in the same way. As the temperature is increased far above the KT transition, the maximum of $|\mathrm{Im}[1/\epsilon(\omega)]|$ approaches the limit value 1/2 (this corresponds to the Drude limit with $\tilde{\epsilon}=1$) as denoted by the horizontal line in (a). The curves seem to develop a plateau as the KT transition is approached from above, as is suggested by the $T=0.95$ curves. As the temperature drops below the KT transition, the amplitude of the flux noise rapidly decreases whereas the characteristic frequency increases, as is illustrated by the curves at $T=0.85$.

this weak increase in a region above the KT transition; the Drude value 1/2 is approached roughly like $\omega^{0.1}$ which explains the discrepancy between exponent 1 and the value 0.9 found in Fig. 6. Thus the existence of a common tangent $1/\omega$ hinges on the weakness of the temperature-dependent factor $T^2/T^{\mathrm{CG}}(T)\tilde{\epsilon}(T)$ which in turn depends somewhat on the details of the system. However, since the temperature dependence of ω_0 is dramatic just above the KT transition, the common tangent should to good approximation exist at least in a limited region above the KT transition.

Below the KT transition there are no free vortices and the response is given by the vortex pairs Eqs. (36) and (37).[15] However, in this case the factor $1/\tilde{\epsilon}\approx 1-1/\epsilon(\omega=0)$ decreases rapidly towards zero as the temperature is decreased below the KT transition.[14] This means that while the characteristic frequency rapidly increases, as the temperature is decreased below the KT transition, the amplitude of the flux noise, which is proportional to $1/\tilde{\epsilon}\approx 1-1/\epsilon(\omega=0)$, rapidly decreases. The KT transition is at $T\approx 0.9$ and already at $T=0.85$ the amplitude of $\omega S(\omega,d)$ has dropped dramatically compared to the almost constant amplitude above the KT transition, as is apparent from Fig. 8(b).

Finally, there is in Fig. 8(b) an indication that the curves develop a plateau as the KT transition is approached from above (compare the curve for $T=0.95$). Such a plateau would suggest that $S(\omega,d)$ is proportional to $1/\omega$ in an intermediate region just above the KT transition. The same development of a plateau can be anticipated in Fig. 8(a) for $|\mathrm{Im}[1/\epsilon(\omega)]|$ and has also been found for the XY model with the time-dependent Ginzburg-Landau dynamics.[14,23]

V. CONCLUDING REMARKS

In the present paper we have explored the fact that the typical experimental setup for measuring the magnetic-flux noise for a superconductor, or JJA, corresponds to the case when the distance d to the pickup coil is much larger than the relevant microscopic lengths. In this limit the flux-noise spectrum and the real part of the conductivity are proportional. This proportionality seems first to have been anticipated in Ref. 7 and has also been experimentally verified.[6] In this paper we have studied this connection in some more detail.

We have also demonstrated that both the shape and the characteristic frequency of the spectrum depend on the distance d to the pickup coil. This means that no detailed conclusions can be drawn from simulations which presumes $d=0$. Furthermore, there is a qualitative difference between the *vorticity*-noise spectrum, which corresponds to discrete events over a sharp boundary, and the *magnetic-flux*-noise spectrum which corresponds to spread-out objects over a boundary. The experimental situation corresponds to a *spread-out magnetic flux* and a pickup coil at a large distance d, which is very different from some earlier simulations which calculated the *vorticity*-noise spectrum for $d=0$.[8,9] Nevertheless the *vorticity*-noise spectrum for $d=0$ has a $\omega^{-3/2}$ tail for higher frequencies which seems to match the experimental results,[4,6] whereas the *magnetic-flux*-noise spectra for $d=0$ does not have such a tail. In accordance with the present simulations, we suggest that the resolution of this dichotomy is that in the large-d limit the magnetic-flux-noise spectrum does have an *intermediate* region with a $w^{-3/2}$ behavior and that it is this intermediate region which is seen in the experiments.

The proportionality between the magnetic-flux-noise spectrum and the real part of the conductivity implies that the noise spectra for a sequence of temperatures just above the KT transition should in a log-log plot have a common tangent with the slope -1. The existence of such a common tangent has also to be verified in experiments,[6] as well as in the present simulations. We also explicitly demonstrated through our simulations that for small d there is no such common tangent.

The existence of a common tangent is by itself not necessarily conclusive. For example, the experimental data for the JJA's in Ref. 5 correspond to the large-d case and the data have indeed a common tangent with slope -1. However, the spectra at a fixed temperature seem to have a $1/\omega$ behavior over a very large region, which differ markedly from the spectra obtained in our simulations for the RSJ model.

The present simulations also suggest that immediately above the KT transition there should be a very small temperature region where the noise spectrum has an intermediate interval with a $1/\omega$ behavior.[23] It has been suggested that the data in Ref. 5 might perhaps be related to this temperature region closest to the transition.[23] However, at the moment there seems to be no accepted explanation for the $1/\omega$ behavior found in Ref. 5.[8]

Finally, we showed that the amplitude of the flux-noise spectrum drops dramatically as the temperature is decreased below the KT transition, and that at the same time the characteristic frequency increases. It should also be possible to observe this effect in experiments.

ACKNOWLEDGMENTS

The authors are grateful to P. Svedlindh and Ö. Festin for discussions of their experimental data and to D. Bormann for discussions of the theory. This work was supported by the Swedish Natural Research Council through Contract No. FU 04040-332.

[1] For a review see, e.g., P. Minnhagen, Rev. Mod. Phys. **59**, 1001 (1987); *Proceedings of the 2nd CTP workshop on Statistical Physics: KT Transition and Superconducting Arrays*, edited by D. Kim, J.S. Chung, and M.Y. Choi (Min-Eum Sa, Seoul, 1993); Physica B **222**, 253(1996).

[2] J.M. Kosterlitz and D.J. Thouless, J. Phys. C **6**, 1181 (1973); V.L. Berezinskii, Zh. Éksp. Teor. Fiz. **61**, 1144 (1971) [Sov. Phys. JETP **34**, 610 (1972)].

[3] M.J. Ferrari, F.C. Wellstood, J.J. Kingston, and J. Clarke, Phys. Rev. Lett. **67**, 1346 (1991).

[4] C.T. Rogers, K.E. Myers, J.N. Eckstein, and I. Bozovic, Phys. Rev. Lett. **69**, 160 (1992).

[5] T.J. Shaw, M.J. Ferrari, L.L. Sohn, D.-H. Lee, M. Tinkham, and J. Clarke, Phys. Rev. Lett. **76**, 2551 (1996).

[6] P. Svedlindh and Ö. Festin (unpublished); M. Björnander, J. Magnusson, P. Svedlindh, P. Nordblad, D.P. Norton, and F. Wellhofer, Physica C **272**, 326 (1996).

[7] J. Houlrik, A. Jonsson, and P. Minnhagen, Phys. Rev. B **50**, 3953 (1994).

[8] I.-J. Hwang and D. Stroud, Phys. Rev. B **57**, 6036 (1998).

[9] P.H.E. Tiesinga, T.J. Hagenaars, J.E. van Himbergen, and J.V. José, Phys. Rev. Lett. **78**, 519 (1997).

[10] K.-H. Wagenblast and R. Fazio, Pis'ma Zh. Éksp. Teor. Fiz. **68**, 291 (1998) [JETP Lett. **68**, 312 (1998)].

[11] C. Timm, Phys. Rev. B **55**, 3241 (1997).

[12] M. Capezzali, Ph.D. thesis, Université de Neuchâtel, 1998.

[13] A. Jonsson and P. Minnhagen, Physica C **277**, 161 (1997).

[14] A. Jonsson and P. Minnhagen, Phys. Rev. B **55**, 9035 (1997).

[15] B.J. Kim, P. Minnhagen, and P. Olsson, Phys. Rev. B **59**, 11 506 (1999).

[16] P. Olsson, Phys. Rev. B **46**, 14 598 (1992).

[17] Note that this only gives a measure of the flux. The magnetic field associated with this flux is spread out; it is strongest in the vortex core region and decays on the length scale Λ.

[18] Note that the circulation of the normal current around a plaquette vanishes since it is proportional to $\Sigma_p(\dot{\theta}_i-\dot{\theta}_j)=0$.

[19] J.D. Jackson, *Classical Electrodynamics*, 2nd ed. (Wiley, New York, 1975).

[20] M. Lax and P. Mengert, J. Phys. Chem. Solids **14**, 248 (1960); R. Voss and J. Clarke, Phys. Rev. B **13**, 556 (1976).

[21] In this respect our results and the ones in Ref. 8 agree completely but differ slightly from Ref. 9 where an exponent somewhat smaller than 3/2 was obtained for the same case (i.e., ≈ 1.2 at $T \gtrsim 1.1$).

[22] In Fig. 4 there appears to be a slight upturn of the spectra at the largest frequencies. As in Ref. 8, this is an artifact of the fast Fourier transformation used in the calculations.

[23] P. Minnhagen, in *Fluctuation Phenomena in High Temperature Superconductors*, Nato ASI Series B, edited by M. Ausloos and A. Varlamov (Kluwer, Netherlands, 1997), p. 279.